Universality, Critical Dynamics, and Vortex Diffusion in Amorphous Mo_3Si Films and $YBa_2Cu_3O_7$ Single Crystals

N.-C. Yeh,[1] D. S. Reed,[1] W. Jiang,[1] U. Kriplani,[1] C. C. Tsuei,[2] C. C. Chi,[2] and F. Holtzberg[2]

[1]*Department of Physics, California Institute of Technology, Pasadena, California 91125*

[2]*IBM, Thomas J. Watson Research Center, Yorktown Heights, New York 10598*

(Received 6 July 1993)

Evidence of a vortex-glass transition in amorphous Mo_3Si films on sapphire is manifested by the universal critical exponents ($\nu \approx \frac{2}{3}$, $z \approx 3$) obtained from dc electrical transport measurements. The exponents are consistent with those found in $YBa_2Cu_3O_7$ single crystals with random point defects, indicating that the vortex-glass transition in both systems belongs to the same universality class. In contrast, ac transport measurements from 100 Hz to 3 MHz suggest that the dominant vortex dynamics in amorphous Mo_3Si thin films is diffusion, and that in $YBa_2Cu_3O_7$ single crystals it is the critical relaxation of thermally induced dislocations.

PACS numbers: 74.60.Ge, 74.25.Dw, 74.72.Bk, 74.76.Db

One of the most fundamental issues associated with the vortex properties of extreme type-II superconductors is the possibility of a "vortex-solid" to "vortex-liquid" melting transition at magnetic fields smaller than the upper critical field [1–5]. While the nature of the vortex-solid phase strongly depends on the defect structure in the superconductor [6–12], the mechanism which drives the melting transition in high-temperature superconductors (HTS) has been attributed to large fluctuations due to the high transition temperatures and the extreme type-II nature [1,2]. Despite the strong possibility of a first-order melting transition in "clean" single crystals [6,7], second-order "vortex-glass" and "Bose-glass" transitions may be common in most HTS systems with random point defects [8–13] and columnar defects [11,14]. To prove the existence of a vortex-glass transition in HTS samples with random point defects, it is necessary to demonstrate that the critical exponents associated with the vortex correlation length and the critical relaxation rate are universal, independent of the magnitude and orientation of the magnetic field, the experimental technique, and the density of point defects. Failing to verify the universality experimentally would either suggest the absence of a second-order phase transition or indicate that experimental variables are not in the right range for detecting such a phase transition. Recent work on $YBa_2Cu_3O_7$ single crystals with random point defects [8–11] has met the requirement of universality by demonstrating universal critical exponents ($\nu \approx \frac{2}{3}$ and $z \approx 3$) and universal functions over two decades of magnetic field, five decades of frequency, and three independent experiments of dc current-voltage characteristics [8,10,11], ac magnetoimpedance [9], and ac magnetic susceptibility [11].

Since conventional amorphous superconductors such as a-Mo_3Si and a-Nb_3Ge films are also extreme type-II superconductors [15] with large compositional disorder, it is natural to ask whether the same type of transition also exists in these materials. In this Letter we provide experimental evidence for a vortex-glass transition in amorphous Mo_3Si films. The phase transition is characterized by the same universal critical exponents as those of $YBa_2Cu_3O_7$ single crystals, suggesting that the vortex-glass transition in two seemingly different superconducting systems belongs to the same universality class. On the other hand, ac transport measurements on both systems at frequencies ranging from 100 Hz to 3 MHz provide evidence for two different type of vortex dynamics; the dominant dynamic process in Mo_3Si films is vortex diffusion, and that in bulk $YBa_2Cu_3O_7$ single crystals is the critical relaxation of thermally induced vortex dislocations [8,9].

Amorphous Mo_3Si films are deposited on sapphire substrates by rf sputtering following the preparation procedure described in Ref. [15]. The sample thickness is $l_t \approx 2000$ Å, surface area $L^2 \sim 15$ mm^2, and the amorphous nature of the sample is confirmed by x-ray diffraction spectroscopy which shows composition modulations at a length scale of ~ 50 Å. The zero-field superconducting transition temperature is $T_c = 7.90$ K, and the resistive transition width is ≤ 15 mK, as shown in the inset of Fig. 1.

Two types of experimental techniques are employed in this work. Measurements of dc current-voltage characteristics are performed by using the standard four-probe technique. Measurements of the amplitude and phase of the ac resistivity (ρ_{ac}) are carried out with a constant-amplitude ac current applied uniformly through the entire thickness of the sample, and the frequencies of the ac current range from 100 Hz to 3 MHz. Details of the ac experimental setup and calibration procedures are given in Ref. [9]. In both types of measurements, the dc magnetic field is applied perpendicular to the plane. Similar measurements have also been performed on a $YBa_2Cu_3O_7$ single crystal [8–10] for comparison.

Figure 2 shows a typical set of the dc electric field (E) versus current density (J) isotherms in a constant magnetic field $H = 2$ kG. If we assume that the vortex-glass melting temperature in a field H is $T_M(H)$ and the transition is second order, the corresponding static and dynamic critical exponents ν and z can be defined as follows

0031-9007/93/71(24)/4043(4)$06.00

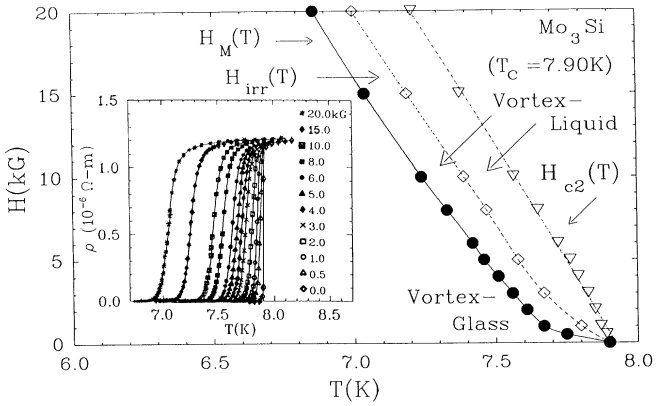

FIG. 1. The vortex phase diagram for a-Mo_3Si films on sapphire. The inset shows the *Ohmic* resistivity of Mo_3Si amorphous films at various constant magnetic fields. The vortex-glass melting line $H_M(T)$ is obtained by scaling the dc E vs J isotherms (see Fig. 2). The irreversible line $H_{irr}(f,T)$ is obtained by identifying the "peak positions" [at $T_{irr}(f,H)$] of the $\mathrm{Im}[\rho_{ac}]$ vs T curves [see Figs. 4(b) and 4(c)]. The upper critical field $H_{c2}(T)$ is estimated by identifying the temperatures at which the condition $\rho(H,T)=0.9\rho(H,T_c)$ is satisfied. The $H_{c2}(T)$ line is consistent with the theoretical fit [18] to the data in Figs. 4(b) and 4(c).

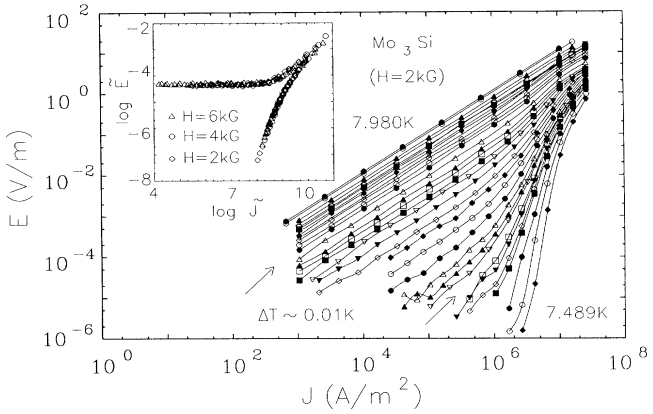

FIG. 2. The electric field (E) versus current density (J) isotherms for $H=2$ kG. The inset shows the universal functions $\tilde{E}\pm$ vs $\tilde{J}$ for $H=2$, 4, 6 kG obtained by using Eq. (2).

[8–10]:

$$\xi_v=\xi_0(H)|1-(T/T_M)|^{-\nu},$$
$$f_T(H,T)=f_c(H)|1-(T/T_M)|^{\nu z}, \quad (1)$$

where ξ_v is the vortex correlation length and f_T is the critical relaxation rate [8,16]. The E vs J isotherms can be scaled into universal functions $\tilde{E}\pm(\tilde{J})$ [8]:

$$\tilde{E}=(E/J)|1-(T/T_M)|^{\nu(d-2-z)},$$
$$\tilde{J}=J|1-(T/T_M)|^{\nu(1-d)}, \quad (2)$$

where d is the dimensionality of the phase transition. The same scaling procedure was performed on seven sets of isotherms taken at seven different magnetic fields ($H=0.5$, 1, 2, 3, 4, 5, and 6 kG). All seven sets of data can be scaled into the same universal functions $\tilde{E}\pm$ using Eq. (2) and the same critical exponents $\nu=0.67\pm0.05$ and $z=3.0\pm0.3$ if $d=3$ is assumed. Three of the seven sets of $\tilde{E}\pm$ taken at magnetic fields $H=2$, 4, 6 kG are shown in the inset of Fig. 2. This demonstration of universality in both the critical exponents and the transport functions lends strong support for the presence of a second-order transition.

To examine the dimensionality of the phase transition, we note that by using the scaling functions $\tilde{E}(\tilde{J})$ and the procedures developed in Ref. [8], the correlation length ξ_0 [see Eq. (1)] in Mo_3Si is found to range from ~20 to ~50 Å for fields from 1 to 25 kG. These values are comparable to the length scale of compositional modulations, and are much smaller than those for $YBa_2Cu_3O_7$ single crystals [8]. As long as $\xi_v < l_c$ which corresponds to temperatures $|T-T_M(H)|\gtrsim0.01$ K ($l_c=2000$ Å is the film thickness), the phase transition associated with the divergence of ξ_v can be justified as three-dimensional. Thus, using Eq. (2) the same critical exponents are obtained for both a-Mo_3Si films and $YBa_2Cu_3O_7$ single crystals, suggesting that the vortex-glass transitions in these two systems belong to the same universality class.

Despite the resemblance of the dc vortex critical phe-

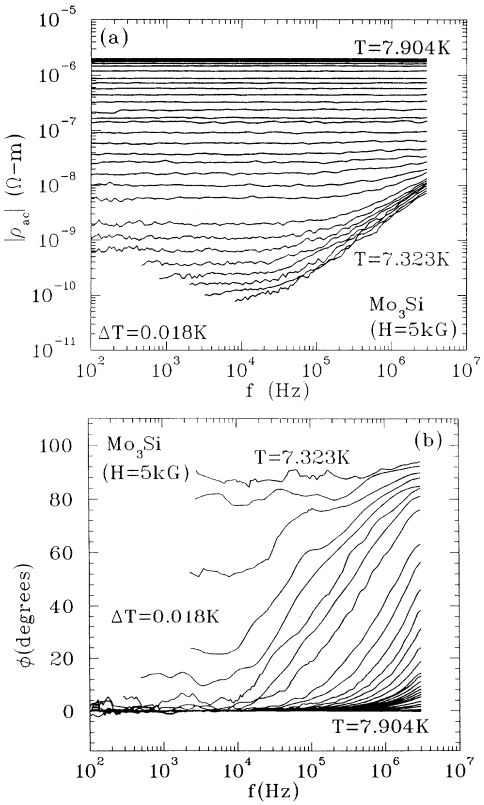

FIG. 3. (a) The amplitude of the ac resistivity $|\rho_{ac}|$ vs f isotherms at $H=5$ kG and (b) the phase [ϕ] vs f isotherms at $H=5$ kG for a-Mo_3Si films.

nomena, there are interesting contrasts between the ac transport properties of a-Mo_3Si films and those of $YBa_2Cu_3O_7$ single crystals as the result of differences in $\xi_0(H)$. The ac measurements on a-Mo_3Si are performed at eight different magnetic fields: $H=0$, 1, 3, 5, 8, 10, 15, and 20 kG. Figures 3(a) and 3(b) show one set of the resistivity amplitude ($|\rho_{ac}|$) and phase (ϕ) versus frequency (f) isotherms for the a-Mo_3Si film in a constant magnetic field $H=5$ kG. The real and imaginary parts of the resistivity for a given frequency can be constructed as a function of the temperature from the data in Figs. 3(a) and 3(b). Figures 4(a) and 4(b) delineate the striking contrasts between the $\mathrm{Im}[\rho_{ac}]$ vs T data for $YBa_2Cu_3O_7$ single crystals and those for a-Mo_3Si films at $H=5$ kG. We find that for each constant frequency, the $\mathrm{Im}[\rho_{ac}]$ data for $YBa_2Cu_3O_7$ single crystals [Fig. 4(a)] are nearly independent of the temperature at $T \lesssim T_M(H)$, and then decrease monotonically with the increasing temperature at $T > T_M(H)$, with the addition of a frequency dependent "peak" at the "irreversible temperature" $T_{irr}(f,H)$. In contrast, the $\mathrm{Im}[\rho_{ac}]$ vs T data for the a-Mo_3Si film peak at the irreversible temperature $T_{irr}(f,H)$ without a monotonically decreasing background. Furthermore, $T_{irr}(f,H)$ is nearly frequency independent for a constant magnetic field, and decreases with the increasing magnetic field for a given frequency, as shown in Figs. 4(b) and 4(c).

The drastic contrast between the ac transport properties of these two superconducting systems may be attributed to the difference in the critical dynamic range [11]: Since the critical relaxtion rate follows $f_T \equiv f_c |1-(T/T_M)|^{vz} \propto \xi_0^{-z} |1-(T/T_M)|^{vz}$, and since ξ_0 is much smaller in a-Mo_3Si films, f_T is expected to be much larger. Thus, the temperature window $\Delta T \equiv T_M (f/f_c)^{1/(vz)}$ for observing the critical dynamics at $f \to f_T$ is much smaller in a-Mo_3Si, because of the smaller T_M and larger f_c. Assuming that $(f_c \xi_0^z) \approx$ const, we find that for $f \sim 10^6$ Hz, $\Delta T \sim 10^{-2}$ K in a-Mo_3Si, compared to $\Delta T \sim 1$ K in $YBa_2Cu_3O_7$. These estimates are consistent with our experimental finding (shown below) that the critical dynamics associated with the vortex-glass transition is only observable in $YBa_2Cu_3O_7$, and that vortex diffusion accounts for the observed ac transport data in a-Mo_3Si.

Let us first consider the diffusion process. Define an external ac current density $\mathbf{J}=Je^{i\omega t}\hat{\mathbf{x}}$ where $\omega=2\pi f$, and assume that the external dc magnetic field is given by $\mathbf{H}=\mathbf{H}_0\hat{\mathbf{z}}$. In the linear response limit, the applied ac current induces a time-dependent surface magnetic induction ($\mathbf{b}$) which satisfies the diffusion equation $(\partial \mathbf{b}/\partial t) = D\nabla^2 \mathbf{b}$, with the diffusion constant given by $D=(\rho_{ac}/\mu_0)$ and the ac resistivity ρ_{ac} given by [2]

$$\rho_{ac} = \mathrm{Re}[\rho_{ac}] + i\,\mathrm{Im}[\rho_{ac}] = i\mu_0\omega\tilde{\lambda}^2 = \mu_0\omega[(-2\lambda_R\lambda_I) + i(\lambda_R^2 - \lambda_I^2)]. \quad (3)$$

In Eq. (3), μ_0 is the permeability in vacuum, λ_R and λ_I are the real and imaginary parts of the effective ac penetration depth $\tilde{\lambda}$ [17],

$$\tilde{\lambda} = \lambda_R + i\lambda_I = \frac{\lambda^2 - i(\tilde{\delta}_{vc}^2/2)}{1+2i(\lambda^2/\delta_{nf}^2)}, \quad (4)$$

λ is the dc penetration depth, δ_{nf} is the normal fluid skin depth [17], and $\tilde{\delta}_{vc}$ is a complex skin depth due to thermally induced vortex depinning [17]. Thus, $\mathrm{Im}[\rho_{ac}]$ yields the following relation:

$$\mathrm{Im}[\rho_{ac}] = \left[\frac{\mu_0\omega(1-\epsilon)}{1+(\omega\tau)^2}\right]\left(\lambda^2 + \frac{B\Phi_0\tau}{\mu_0\eta}\right) \times \frac{1}{[1+(2\lambda^2/\delta_{nf}^2)^2]}, \quad (5)$$

where η denotes the viscosity, Φ_0 the flux quantum, $\epsilon \equiv [I_0(\mu)]^{-2}$ the flux-creep factor, $\tau \equiv (\eta/k_p)[I_0^2(\mu) - 1]/[I_0(\mu)I_1(\mu)]$ the flux-creep relaxation time [17], $\mu \equiv U_p/(2k_BT)$, k_p the spring constant, U_p the pinning potential, and I_0, I_1 the zeroth and the first-order modified Bessel functions.

Equation (5) predicts that $\mathrm{Im}[\rho_{ac}]$ reaches a maximum when $\omega=\omega^* \equiv (1/\tau)$. The theoretical curves obtained by

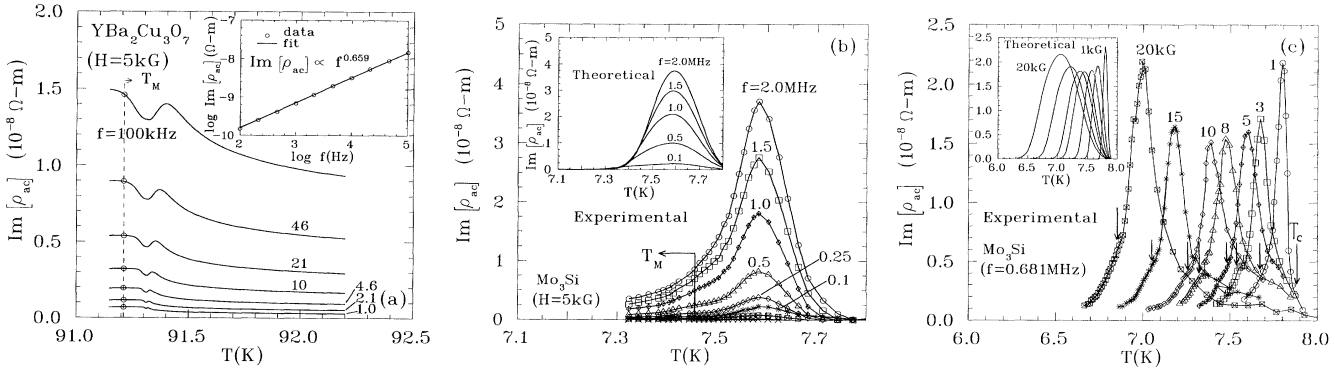

FIG. 4. (a) $\mathrm{Im}[\rho_{ac}(f,H,T)]$ vs T curves for $YBa_2Cu_3O_7$ single crystals at various constant frequencies and $H=5$ kG. The inset shows that the frequency dependence $\{\mathrm{Im}[\rho_{ac}] \propto f^{0.659}\}$ at $T=T_M(H)=91.21$ K is consistent with the scaling relations in Eq. (6). (b) $\mathrm{Im}[\rho_{ac}(f,H,T)]$ vs T curves for a-Mo_3Si films at various constant frequencies and for $H=5$ kG. The inset shows the corresponding theoretical curves obtained by using Eq. (5). (c) $\mathrm{Im}[\rho_{ac}(f,H,T)]$ vs T curves for a-Mo_3Si films at various fields and for a constant frequency $f=0.681$ MHz. The inset shows the theoretical curves obtained by using Eq. (5).

using Eq. (5) for a-Mo_3Si films are shown in the insets of Figs. 4(b) and 4(c). Note that a semiquantitative agreement with the experimental data can be achieved [18], although the widths of the high-field theoretical curves are generally broader than those of the experimental data. We also note that for a given magnetic field, the diffusion-related irreversible temperature $T_{irr}(H)$ is always higher than the vortex-glass temperature $T_M(H)$, as shown in Figs. 4(b) and 4(c), and the H vs T phase diagram in Fig. 1. Since the diffusion model does not include direct reference to a phase transition, it is only applicable to the data in the vortex-liquid state.

In the case of $YBa_2Cu_3O_7$ single crystals, the current-induced ac magnetic field is limited to the surface of the sample because the sample thickness (~ 20 μm) is much larger than the penetration depth (~ 1400 Å). Thus, the dominant contribution to the ac resistivity results from direct interactions between the bulk ac current and the thermally induced vortex dislocations. The corresponding ac resistivity near $T_M(H)$ is governed by the scaling relations [8,9],

$$\rho_{ac}(f,H,T) \sim |1-(T/T_M)|^{\nu(2-d+z)} \tilde{\rho}_{\pm}(\tilde{f}) ,$$
$$\tilde{f} = f|1-(T/T_M)|^{-\nu z} , \quad (6)$$

where $\tilde{\rho}_+$ and $\tilde{\rho}_-$ denote the universal functions for $T > T_M$ and $T < T_M$, respectively. In Ref. [9] we have shown that the ac resistivity of $YBa_2Cu_3O_7$ single crystals is consistent with the critical scaling relations in Eq. (6). Therefore the frequency dependence of $\mathrm{Im}[\rho_{ac}]$ in Fig. 4(a) can be understood in the context of critical phenomena: Since $\mathrm{Im}[\rho_{ac}] = |\rho_{ac}|\sin\phi_c$ with $\phi_c = (\pi/2)(1-1/z)$ being the critical phase at $T_M(H)$ [9,16], and since the amplitude of the ac resistivity at $T_M(H)$ follows the frequency dependence $|\rho_{ac}| \sim f^{1-(1/z)}$ [4,9], we find that the theoretical magnitude of $\mathrm{Im}[\rho_{ac}]$ increases with the increasing frequency near $T_M(H)$, consistent with the experimental data in Fig. 4(a). The inset in Fig. 4(a) shows the logarithmic plot of $\mathrm{Im}[\rho_{ac}]$ vs f for $T = T_M(H)$ and $H = 5.0$ kG. Note that the slope is equal to $(1-1/z)$, and that the experimental data yield $\mathrm{Im}[\rho_{ac}] \propto f^{0.659}$ at $T_M(H) = 91.21$ K, consistent with the fact that $z \approx 3.0$. We therefore conclude that the dominant contribution to ρ_{ac} in $YBa_2Cu_3O_7$ single crystals is related to the critical dynamics of the vortex-glass transition.

Finally, we note that for $T > T_M(H)$, the ac surface magnetic fields in $YBa_2Cu_3O_7$ single crystals also give rise to small, diffusion-related "peaks" in the $\mathrm{Im}[\rho_{ac}]$ vs T data [Fig. 4(a)], indicating that the theory of vortex depinning becomes relevant if the temperature is outside of the critical regime of the vortex-glass transition. Consequently, a complete theoretical description for $\rho_{ac}(f,T,H)$ must include both critical dynamics and vortex diffusion to fully account for the experimental data. This issue still awaits further investigations.

In summary, we have provided experimental evidence for a vortex-glass transition in amorphous Mo_3Si films by deriving universal critical exponents ($\nu \approx \frac{2}{3}$ and $z \approx 3$) and universal functions from dc transport measurements. The critical exponents for a-Mo_3Si films are consistent with those for $YBa_2Cu_3O_7$ single crystals, indicating that the vortex-glass transition in both systems belongs to the same universality class. In contrast, ac transport measurements from 10^2 to 3×10^6 Hz suggest that critical dynamics associated with the vortex-glass transition is only observable in $YBa_2Cu_3O_7$ single crystals, because of the much smaller critical dynamic range in a-Mo_3Si films which prevents direct observation of frequency-dependent critical phenomena.

This work is jointly supported by ONR Grant No. N00014-91-J-1556, the David and Lucile Packard Foundation, IBM-Caltech Cooperative Research Fund, and NASA/OACT. We thank Nils Asplund for technical assistance.

[1] D. R. Nelson and H. S. Seung, Phys. Rev. B **39**, 9153 (1989); M. C. Marchetti and D. R. Nelson, Phys. Rev. B **41**, 1910 (1990).
[2] E. H. Brandt, Phys. Rev. Lett. **63**, 1106 (1989); Int. J. Mod. Phys. B **5**, 751 (1991).
[3] N.-C. Yeh, Phys. Rev. B **40**, 4566 (1989); **42**, 4850 (1990).
[4] D. S. Fisher, M. P. A. Fisher, and D. Huse, Phys. Rev. B **43**, 130 (1991).
[5] N.-C. Yeh, Phys. Rev. B **43**, 523 (1991).
[6] R. E. Hetzel, A. Sudbo, and D. A. Huse, Phys. Rev. Lett. **69**, 518 (1992).
[7] H. Safar *et al.*, Phys. Rev. Lett. **69**, 824 (1992).
[8] N.-C. Yeh *et al.*, Phys. Rev. B **47**, 6146 (1993); Mat. Res. Soc. Symp. Proc. **275**, 169 (1992).
[9] D. E. Reed *et al.*, Phys. Rev. B **47**, 6150 (1993); Mat. Res. Soc. Symp. Proc. **275**, 413 (1992).
[10] W. Jiang *et al.*, Phys. Rev. B **47**, 8308 (1993); Mat. Res. Soc. Symp. Proc. **275**, 789 (1992).
[11] N.-C. Yeh *et al.*, Physica A (to be published).
[12] P. L. Gammel, L. F. Schneemeyer, and D. J. Bishop, Phys. Rev. Lett. **66**, 953 (1991).
[13] R. H. Koch *et al.*, Phys. Rev. Lett. **63**, 1511 (1989).
[14] D. R. Nelson and V. M. Vinokur, Phys. Rev. Lett. **68**, 2398 (1992); Phys. Rev. B **48**, 13060 (1993).
[15] R. Wordenweber, P. H. Kes, and C. C. Tsuei, Phys. Rev. B **33**, 3172 (1986).
[16] A. T. Dorsey, Phys. Rev. B **43**, 7575 (1991).
[17] M. Coffey and J. R. Clem, Phys. Rev. Lett. **67**, 386 (1991); Phys. Rev. B **46**, 11757 (1992).
[18] The material parameters employed for the theoretical curves in the insets of Figs. 4(b) and 4(c) are $U_p = U_0|1-(T/T_c)|^{1.5}/H$ [17], H is measured in T, $U_0 = 125$ meVT, and $U_p = 0$ for $T > T_c$; $\eta = H_{c2}(T)\Phi_0/(\epsilon\rho_n)$, $H_{c2}(T) = H_{c2}(0)|1-(T/T_c)^2|$, $H_{c2}(0) = 12$ T; $k_p(T,H) = k_p(0)|1-(T/T_c)^2|^2\{1-[H/H_{c2}(0)]\}^2$, $k_p(0) = 25$ N/m^2; and $\rho_n = 1.2\times10^{-6}$ Ω m as well as $T_c = 7.90$ K are derived empirically.